Simultaneously Harvesting Electrostatic and Mechanical Energies from Flowing Water by a Hybridized Triboelectric Nanogenerator

Gang Cheng,[†,‡,⊥] Zong-Hong Lin,[†,⊥] Zu-liang Du,[‡] and Zhong Lin Wang[†,§,*]

[†]School of Material Science and Engineering, Georgia Institute of Technology, Atlanta, Georgia 30332-0245, United States, [‡]Key Lab for Special Functional Materials, Henan University, Kaifeng 475004, China, and [§]Beijing Institute of Nanoenergy and Nanosystems, Chinese Academy of Sciences, Beijing 100083, China. [⊥]These authors contributed equally to this work.

ABSTRACT Flowing water contains not only mechanical kinetic energy, but also the electrostatic energy owing to the triboelectric charges caused by its contact with surrounding media such as air. In this paper, a water wheel hybridized triboelectric nanogenerator (TENG), composed of a water-TENG part and a disk-TENG part, has been developed for simultaneously harvesting the two types of energies from the tap water flowing from a household faucet. The wheel blades of the hybridized TENG are composed by superhydrophobic polytetrafluoroethylene (PTFE) thin films with nanostructures, which are used as water-TENG to harvest the electrostatic energy from the flowing water. In addition, the flowing water impacted on the wheel blades also causes the rotation motion of disk-TENG and can be used to harvest the mechanical kinetic energy. The short-circuit current of the water-TENG and the disk-TENG at a flowing water rate of 54 mL/s can reach 12.9 and 3.8 μA, respectively. The hybridized TENG is also demonstrated to harvest wind energy and acts as a self-powered sensor to detect the flowing water rate and wind speed. All these results show the potentials of the hybridized TENG for harvesting multiple types of energies from the environment.

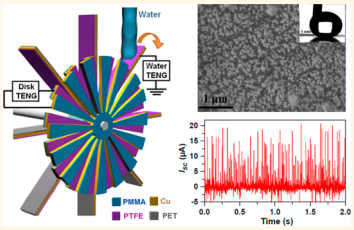

KEYWORDS: triboelectric nanogenerator · flowing water · self-powered sensor

Harvesting mechanical energy from ambient environment and human body has attracted increasing interest for building self-powered electronic devices and large-scale energy needs.[1−4] The mechanical energy can be transformed into electricity based on various physical mechanisms, such as electromagnetic,[5,6] electrostatic,[7,8] and piezoelectric effects.[9−15] Recently, triboelectric nanogenerator (TENG)[16−28] has been invented as a new technology to harvest mechanical energy, which is based on contact electrification effect and electrostatic induction.[29−31] When two triboelectric surfaces (tribo-surfaces) with opposite triboelectric charges (tribo-charges) are periodically contacted and separated, the potential difference between the metal electrodes of the two tribo-surfaces periodically varies, which drives the electrons to flow between the two metal electrodes. Various applications of TENG have been demonstrated, such as self-powered chemical sensor,[32,33] electrodegradation,[34] and powering commercial light emitting diodes (LED).[21−25]

For traditional TENG, two solid materials are contacted together to generate tribo-charges on their interface.[16−28] Recently, the tribo-charges on the water/solid[35] and water/air[36] interfaces are used to develop a water-based TENG, which demonstrate promising applications of TENG for harvesting energy from flowing water and ocean wave. The flowing water carries two types of energies. One is the mechanical energy of the motion of the flowing water. The second is the electrostatic energy, which comes from the tribo-charges in water generated during its traveling processes in pipe and/or air due to the contact electrification.[37] In our previous report, a water-TENG has been developed to harvest the electrostatic energy from the water drop.[36] To simultaneously harvest the electrostatic and mechanical energies from the flowing water, a hybridized TENG with a water wheel structure has been developed in this paper, which is

* Address correspondence to zlwang@gatech.edu.

Received for review December 23, 2013 and accepted January 23, 2014.

Published online January 27, 2014
10.1021/nn406565k

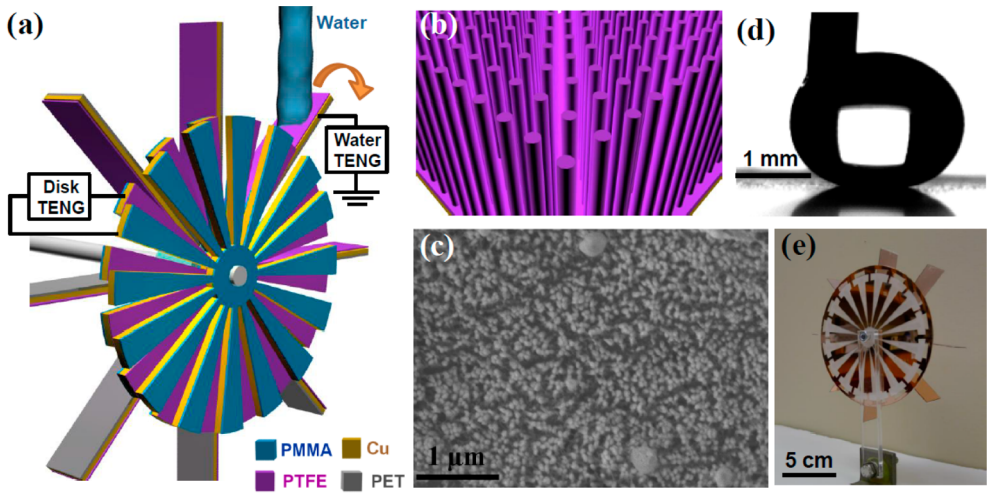

Figure 1. (a) The structure diagram of the hybridized TENG. The structure diagram (b), the SEM image (c), and the contact angle (d) of the PTFE thin film with nanostructure. (e) The photography of the prepared hybridized TENG.

composed by two parts: a water-TENG and a disk-TENG. The wheel blades are composed by superhydrophobic polytetrafluoroethylene (PTFE) thin films with nanostructures, which are used as the water-TENG to harvest the electrostatic energy from flowing water. In addition, the flowing water impacted on the wheel blades also causes the rotation motion of disk-TENG and harvests the mechanical kinetic energy. The open-circuit voltages of the water-TENG and the disk-TENG are around 72 and 102 V, respectively, and their short-circuit currents are around 12.9 and 3.8 μA, respectively. It is also demonstrated that the water wheel TENG can harvest energy from wind and act as self-powered sensors for detecting flowing water rate and wind speed.

RESULTS AND DISCUSSION

The structure diagram of the hybridized TENG with a water wheel structure is shown in Figure 1a, which consists of two different types of TENGs: one is the water-TENG and the other is the disk-TENG. The water-TENG is composed of 8 wheel blades and operates as a single-electrode-based TENG[27,28] to harvest the electrostatic energy from flowing water, in which the electrical channel is formed between the Cu electrode on each blade and the ground. The disk-TENG is composed by two disks, a back disk and a front disk, and each disk has 16 segments. The water wheel structure is assembled using a smooth metal rod as a rotation axis through the centers of the wheel and the two disks. The back disk is connected with the wheel, and the wheel blades are also used to gather the flowing water force to drive the rotation of the wheel and the back disk. The front disk is fixed on the rotation axis and keeps motionless even during the whole process. The disk-TENG is used to harvest the mechanical energy of the water, in which the electrical channel is formed between the Cu electrodes of the two disks. For fabricating the blades, a 100-nm thin Cu film was deposited on a square polyethylene terephthalate (PET) sheet to serve as the electrode layer, and then a PTFE film with nanostructures fabricated by using porous anodic Al oxide (AAO) as template was attached onto the Cu electrode using a double-sided tape. The Cu electrodes of the 8 blades were electrically connected together. Two poly(methyl methacrylate) (PMMA) sheets were first processed by laser cutting to form the 16-segment-structured circle disks as the substrates of the disk-TENG. For the back disk, a 100-nm thin Cu film was deposited on one PMMA substrate, and then a PTFE film with nanostructures was attached onto the Cu electrode. For the front disk, another 100-nm thin Cu film was deposited on the other PMMA substrate and directly used as the contact material. The PTFE layer of the back disk and the Cu layer of the front disk were brought to a face-to-face intimate contact to form a sliding TENG operating at rotation disk mode.[25]

The surface of PTFE film on the wheel blades of water-TENG and the back disk of disk-TENG is fully covered by high-density PTFE nanorods (Figure 1b). The mean length and diameter of the PTFE nanorods are 360 and 45 nm from the SEM image displayed in Figure 1c. The contact angle of the PTFE film is 162° (Figure 1d), which represents the surface of the PTFE film is superhydrophobic. The high-density nanorods covered on the surface will contain trapped air and reduce the actual contact area between the surface and water droplets, which causes the superhydrophobic ability of the PTFE film. The superhydrophobic ability on the surface of the wheel blades is a critical factor for the performance of the water-TENG, which will be discussed later. In addition, the nanostructures on the PTFE surface will also increase the effective contact area of the two tribo-surfaces and enhance the electrical output of the disk-TENG.[21] The photograph of the prepared hybridized TENG is shown in Figure 1e.

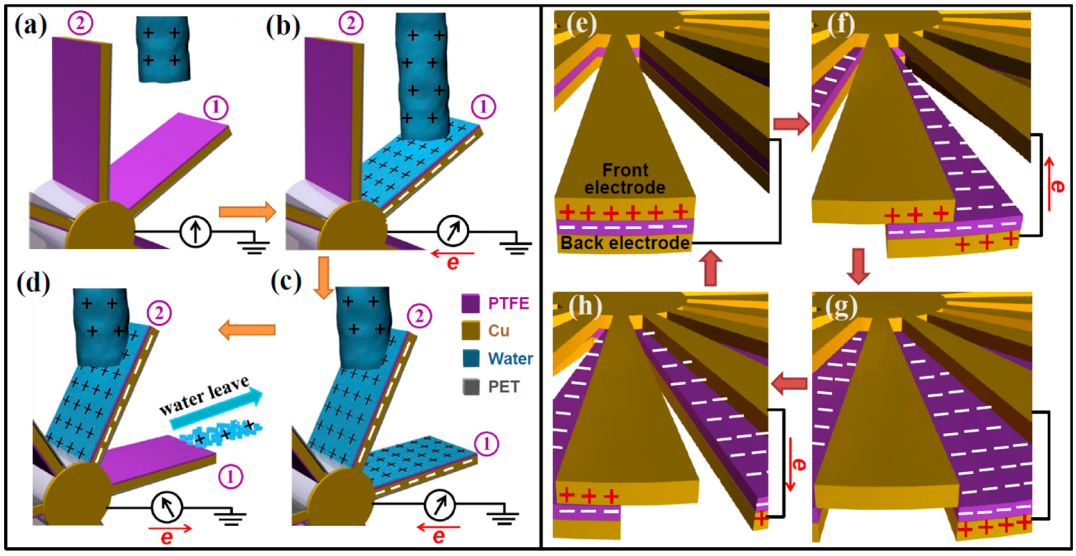

Figure 2. The working mechanism of the water-TENG part (a–d) and the disk-TENG part (e–h) of the hybridized TENG.

It is necessary to mention that we will place a PET sheet between the wheel blades of water-TENG and the back disk of disk-TENG to prevent the disk-TENG from water when the hybridized TENG is working. However, for the purpose of clearly showing the whole structure of the hybridized TENG, the PET sheet here is not shown in the structure diagram (Figure 1a) and photography (Figure 1e) of the hybridized TENG.

In our experiment, the tap water flowing from a common household faucet was used to drive the hybridized TENG. The working mechanism of the water-TENG part of the hybridized TENG is schematically shown in Figures 2a–d. According to our previous investigation,[36] the tap water flowing from the faucet has positive tribo-charges due to the contact electrification between the water and the pipe/air during its traveling processes, as shown in Figure 2a. As the flowing water reaches the blade-1, a positively charged water film is formed on the PTFE surface of the blade-1, because of the tribo-charges created between the water and the water pipe. As a result, a positive potential difference is created between the Cu electrode of the blade-1 and the ground, which will drive the electrons to transfer from the ground to the Cu electrode of the blade-1 and generate a positive current until the potential difference is decreased to zero (Figure 2b). Because the flowing water impacted on the blade-1 will also cause the rotation of wheel, next the flowing water will contact the blade-2. Then another positively charged water film will form on the PTFE surface of the blade-2, and consequently, another positive potential difference is created between the Cu electrode of the blade-2 and the ground, attributing a positive current until the potential difference is decreased to zero (Figure 2c). After this, the water film with its positive charges is moving off the PTFE surface of blade-1 due to the continuous rotation of wheel blades and superhydrophobic property of the surface. With the removal of the water film on the blade-1, a negative potential difference is generated between the Cu electrode of blade-1 and the ground because of the negative charges on the Cu electrode, which drives the electrons to transfer from the Cu electrode to the ground and generates a negative current until the potential difference becomes zero, as shown in Figure 2d. With the continuous rotation of the wheel blades, the water reaches different blades in sequence, and alternative positive and negative currents are generated with similar processes as shown in Figure 2c,d. For enhancing the output performance of the water-TENG, it is required that the water film on the surface of one blade can be fully removed as the flowing water reaches the other blades. The superhydrophobicity of the PTFE film on the blades plays a key role for the removal of the water film and enhances the electrical output of the water-TENG, which will be demonstrated later.

The working mechanism of the disk-TENG part of the hybridized TENG is schematically drawn in Figure 2e–h. In the initial stage, the back disk and the front disk are fully contacted, and the positive and negative tribo-charges are generated on the Cu surface of the front disk and the PTFE surface of the back disk, respectively, since PTFE has stronger tendency to gain electrons than Cu in the triboelectric series (Figure 2e). At this stage, the positive and negative charges are fully overlapped, and thus, there is no potential difference between the Cu electrodes of the two disks and no current is generated. With the rotation of the back disk, the two disks are partly separated, and a positive potential difference on the front electrode is formed, which drives the electrons to flow from the back electrode to the front electrode and generates a positive current, as shown in Figure 2f. As the two disks

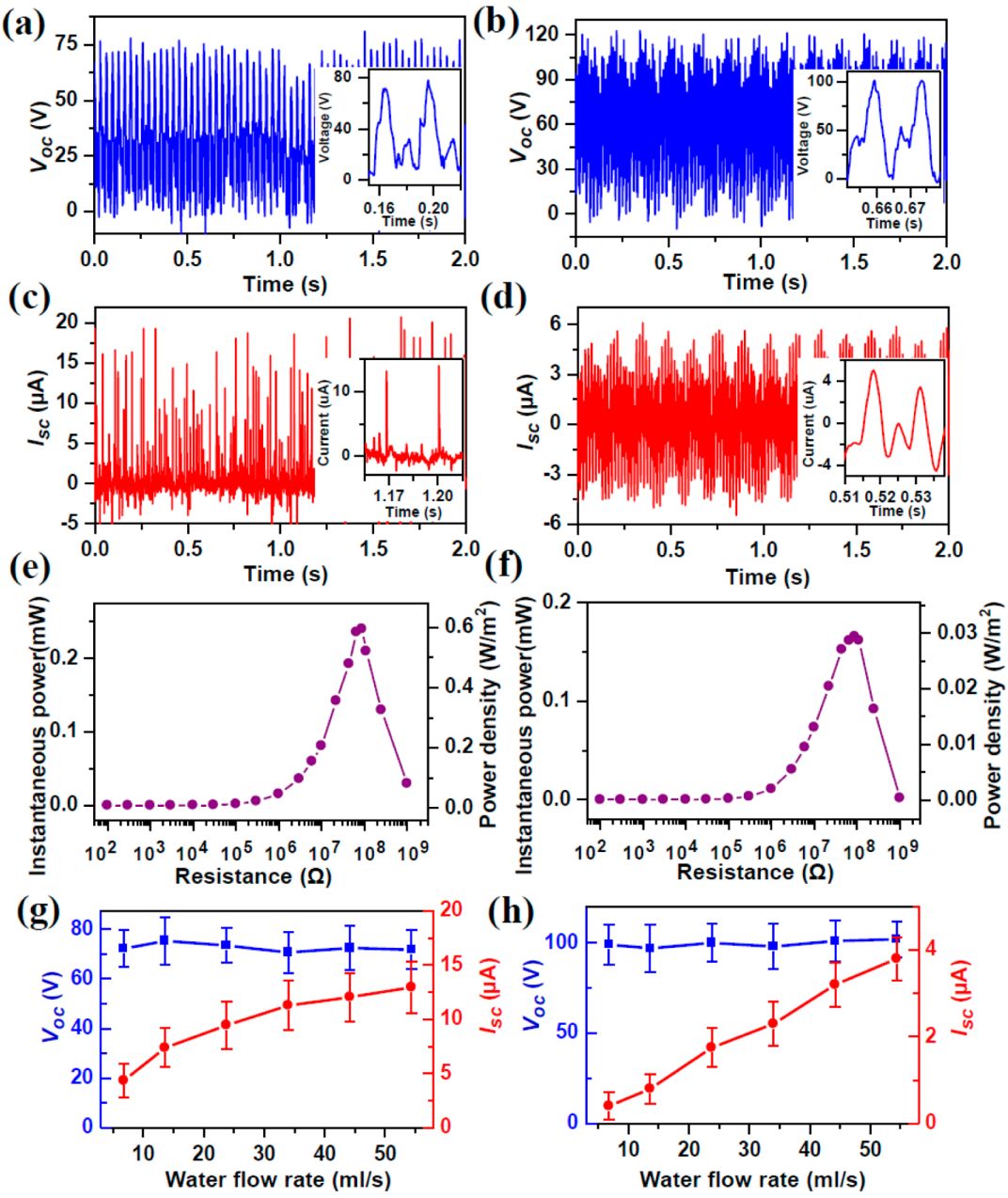

Figure 3. The V_{oc} curves of the water-TENG (a) and the disk-TENG (b). The I_{sc} curves of the water-TENG (c) and the disk-TENG (d). The dependences of the instantaneously maximum power and power density on the load resistance of the water-TENG (e) and the disk-TENG (f). The dependences of the V_{oc} and I_{sc} values on the flowing water rate of the water-TENG (g) and the disk-TENG (h).

are fully separated, the induced positive charges on the back electrode reach their maximum value, and the net charges on the front electrode nearly decrease to zero (Figure 2g). As the back disk continues rotating, the front electrode begins to get in contact with the PTFE film of another adjacent segment of the back disk, and then a negative potential difference is formed on the front electrode, which drives the electrons to flow from the front electrode to the back electrode and generates a negative current, as shown in Figure 2h. Next, the two disks are fully contacted again, and the induced charges in the back electrodes are fully flowed to the front electrode, as shown in Figure 2e. With the further rotation of the back disk, another cycle similar to the processes from Figure 2e–h will start.

For measuring the electrical output properties of the hybridized TENG, the tap water flowing from a household faucet at a flow rate of 54 mL/s was used to drive the hybridized TENG, and the vertical distance between the water outlet of the faucet and the rotation axis of the hybridized TENG is around 25 cm. The curves of the open-circuit voltage, V_{oc}, of the water-TENG and the disk-TENG are shown in Figure 3, panels a and b, respectively, and their magnification curves are shown

in the insets. The V_{oc} values of the water-TENG and the disk-TENG are around 72 and 102 V, respectively. The positive V_{oc} value of the water-TENG indicates the positive tribo-charges in the flowing water from the household faucet, which is in agreement with our previous report.[36] The curves of the short-circuit current (I_{sc}) of the water-TENG and the disk-TENG are shown in Figure 3, panels c and d, respectively, and their magnification curves are shown in the insets. The I_{sc} values of the water-TENG and the disk-TENG are around 12.9 and 3.8 μA, respectively. By integrating the absolute values of the I_{sc} curve of the water-TENG, it is calculated that the collected charge in a unit time is 0.68 μQ/s; therefore, the carried tribo-charge in the flowing water in a unit time is 0.34 μQ/s, and the corresponding tribo-charge density in the flowing water from faucet is 6.3 nQ/mL. The mean interval time between two positive current peaks of the water-TENG and the disk-TENG are around 0.03 and 0.015 s, respectively, and the corresponding output frequencies are 33.3 and 66.7 Hz, respectively. The output frequency of the TENG with multiple segments can be expressed by $f = nN/60$, where n is the number of the divided segments in the TENG and N is the rotation speed in a unit of rounds per minute (rpm). According to this equation, the rotation speed of the hybridized TENG at a flowing water rate of 54 mL/s is around 249 rpm. Since the two parts of the hybridized TENG have the same rotation speed and the segment number of the disk-TENG (16) is two times of magnitude than that of the water-TENG (8), the output frequency of the disk-TENG is two times the magnitude of that for the water-TENG. Increasing the segment number in the disk and the blades number in the wheel blades can increase the output frequency of the disk-TENG and water-TENG, respectively.

For the water-TENG, the positive and negative current peaks correspond to the processes of the formation and the removal of the positively charged water film on the blade surface, respectively. As shown in Figure 3c, the positive current peak of the water-TENG is remarkably higher than the negative current peak, which indicates that the removal process of the water film requires longer time than the formation process. In the control experiment, the superhydrophobic PTFE film on the blades was replaced by a hydrophilic nylon film and a hydrophobic smooth PTFE film without nanorods to test the effect of the superhydrophobicity on the output performance of the hybridized TENG. With the use of a nylon film in the blade surface and the same experiment conditions, the periodically sharp current peaks disappear and only some irregular peaks around 0.4 μA are present (Figure S1a). With the use of a smooth PTFE film of contact angle about 120° and the same experiment conditions, the I_{sc} peaks of the water-TENG decrease about 60% compared to those using superhydrophobicity PTFE film with nanorods (Figure S1b). Meanwhile, the I_{sc} curve of the disk-TENG (Figure S1c) nearly keeps the same as that using the superhydrophobicity PTFE film with nanorods in the blades. The comparison results indicate that superhydrophobic surface of the blades plays a critical role for the removal of the water film on the blade surface and is helpful for enhancing the output performance of the water-TENG. Since the disk-TENG is design to harvest the mechanical energy of the flowing water, its output performance is independent of the hydrophobic property of the blades surface.

To investigate the output power of the water wheel TENG at an external load resistor, the output voltage and output current of the water-TENG and the disk-TENG at various load resistances ranging from 100 Ω to 1 GΩ were measured, and the corresponding output power value at each resistance was calculated using $P = IV$. The dependences of the output voltage and output current of the water-TENG and the disk-TENG on the load resistance are shown in Figure S2. Figure 3e,f shows the dependences of the instantaneously maximum output power and the corresponding power density (the output power per contact area of the TENG) of the water-TENG and the disk-TENG, respectively. For the water-TENG, the instantaneously maximum power of 0.24 mW appears at a load of 88 MΩ, and the corresponding instantaneously maximum power density is 0.59 W/m^2. For the disk-TENG, the instantaneously maximum power of 0.17 mW appears at a load of 88 MΩ, and the corresponding instantaneously maximum power density is 0.03 W/m^2. The V_{oc} and I_{sc} of the water-TENG and the disk-TENG at various flowing water rates ranging from 7 to 54 mL/s were measured. The dependences of V_{oc} and I_{sc} on the flowing water rate for the water-TENG are shown in Figure 3g, in which V_{oc} values nearly keep constant around 72 V for various flow rates, and the I_{sc} value increases from 4.3 to 12.9 μA as the flowing water rate increases from 7 to 54 mL/s. The increase of the I_{sc} is caused by more tribo-charges carried in the flowing water in a unit time at higher flowing rate. The dependences of V_{oc} and I_{sc} on the flowing water rate for the disk-TENG are shown in Figure 3h, in which V_{oc} values nearly keep constant around 101 V for various flowing rates, and the I_{sc} value nearly increases linearly with the flowing water rate. For TENG operating at the rotation disk mode, the I_{sc} values will increase linearly with the rotation speed of the disk, which has been discussed in detail in our previous report.[25] As shown in Figure S3, the rotation speed of the hybridized TENG increases linearly with the flowing water rate, which is the reason for the linear increase of the I_{sc} values of the disk-TENG. This linear dependence of the I_{sc} value on the flowing water rate demonstrates its potential application as a self-powered sensor for detecting flowing water rate.

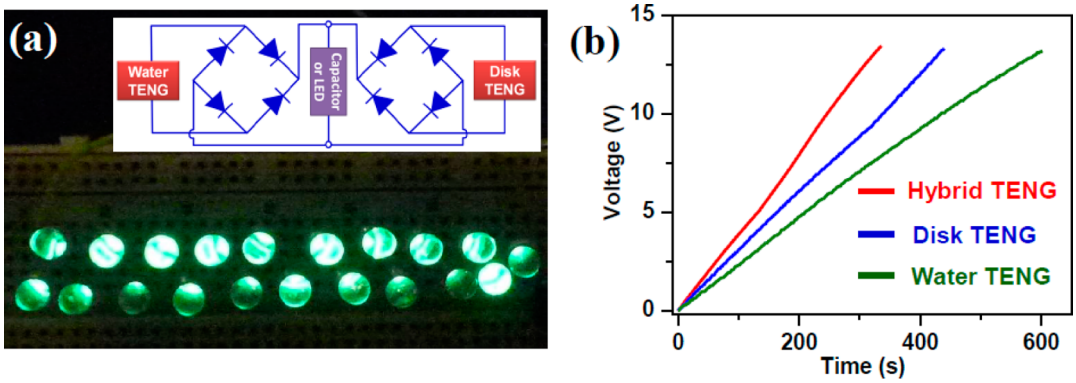

Figure 4. (a) The photography of 20 commercial LED bulbs driven by the hybridized TENG at a flowing water rate of 54 mL/s, and inset shows the diagram of the rectifying circuit. (b) The measured voltage of a 4.7 μF capacitor charged by the hybridized TENG and a single part of the hybridized TENG at a flowing water rate of 54 mL/s.

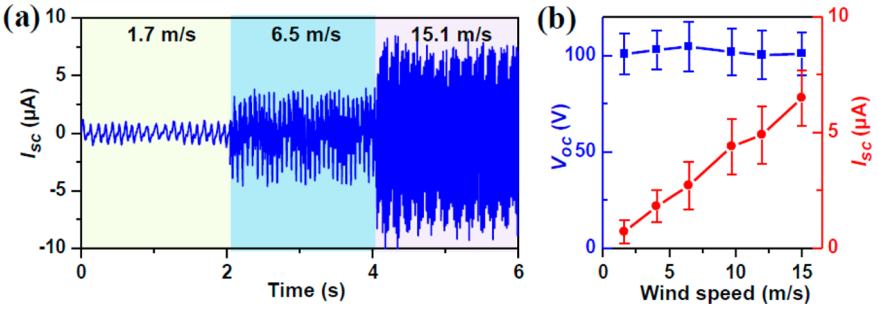

Figure 5. The I_{sc} curve at various wind speeds (a) and the dependences of V_{oc} and I_{sc} values on wind speed (b) of the disk-TENG when it is driven by wind.

For practical applications in driving LEDs or charging a capacitor, the electrical outputs of the water-TENG and the disk-TENG are connected in parallel after they are converted to pulse output in the same directions by using two full-wave rectifying bridges, as shown in the inset of Figure 4a. As the hybridized TENG is driven by water at a flow rate of 54 mL/s, 20 commercial green LEDs are lighted up, as shown in Figure 4a. The hybridized TENG is also demonstrated to charge a capacitor of 4.7 μF at a flowing water rate of 54 mL/s, and the voltage curves of the capacitor are shown in Figure 4b. When the capacitor is charged by the rectified output of water-TENG and the rectified output of disk-TENG, respectively, it takes about 596 and 435 s to charge the capacitor to a voltage of 13 V, respectively. When using the total hybridized TENG, it takes 326 s to charge the capacitor to a voltage of 13 V.

Since the rotation of the wheel blades can also be driven by wind, the hybridized TENG can be used to harvest the wind energy, which will further expands its applications. The wind with various speeds is used to drive the rotation of the disk-TENG, and the measured I_{sc} curve of the disk-TENG is shown in Figure 5a. With the increase of the wind speed, the output frequency and I_{sc} value remarkably increase. The dependences of the V_{oc} and I_{sc} values of the disk-TENG on the wind speed ranging from 1.7 to 15.1 m/s are shown in Figure 5b, in which the V_{oc} value nearly keeps constant around 101 V for various wind speeds, and the I_{sc} value nearly increases linearly with the wind speed. As shown in Figure S4, the rotation speed of the disk-TENG increases linearly with the wind speed, and this causes the linear increase of the I_{sc} value based on the similar reason discussed in Figure 3h.[25] The linear dependence of the I_{sc} values on the wind speed demonstrates its potential application as a self-powered sensor for detecting wind speed. When the hybridized TENG is used to harvest wind energy, only the disk-TENG can generate electric energy, and the function of the wheel blades of the water-TENG is converting the wind energy to the mechanical rotation motion of the back disk. In this case, there is no electrical output for the water-TENG part (shown in Figure S5), because the flowing water with tribo-charges is a necessary condition to generate electrical output for the water-TENG.

CONCLUSION

In summary, a water wheel based hybridized TENG, including a water-TENG and a disk-TENG, has been developed for simultaneously harvesting the electrostatic and mechanical energies from the flowing water. The water-TENG is composed of wheel blades with superhydrophobic surfaces covered by the PTFE nanostructures, which operate as single-electrode-based TENG to harvest the electrostatic energy from water. The disk-TENG is composed of two disks, and one disk

rotates together with the wheel blades under the impact of flowing water, which operates as a rotation disk mode TENG to harvest the mechanical energy from water. At a flowing water rate of 54 mL/s, the open-circuit voltage of the water-TENG and the disk-TENG is around 72 and 102 V, respectively, their short-circuit current is around 12.9 and 3.8 μA, respectively, and their instantaneously maximum power density is 0.59 and 0.03 W/m^2, respectively. We also demonstrated that the hybridized TENG can be used to harvest energy from wind. The short-circuit current of the disk-TENG is linearly proportional to the flowing water rate and the wind speed, which shows the potential applications of the hybridized TENG as self-powered sensors for detecting flowing water rate and wind speed. The hybridized TENG provides a novel approach to harvest multiple types of energies from the environment.

METHODS

Fabrication of the Nanostructured PTFE Film. First, microstructures were fabricated by blasting an Al foil with sand particles using compressed air. The sand-blasted Al foil was further anodizing in a 0.3 M oxalic acid solution to obtain an anodic Al oxide (AAO) template with nanometer-sized holes. The SEM image of the AAO template is shown in Figure S6, and the average diameter of the holes in the AAO template is about 45 nm. Then the PTFE solution was poured into the AAO template and a conventional vacuum process was applied to remove the air remaining in the nanoholes. After the curing at ambient temperature for one day, the solvent was evaporated and leaved a PTFE thin film with nanostructures. Finally, the PTFE thin film was peeled off from the AAO template using a double-sided tape.

Fabrication of the TENG. First, the PMMA sheet (thickness of 3 mm) and the PET sheet (thickness of 0.5 mm) were processed by laser cutting (PLS6.75, Universal Laser Systems) to serve as the substrates of the two disks and the eight blades, respectively. And then, the Cu films of thickness of 100 nm were deposited on these substrates by e-beam evaporator. After that, the PTFE films with nanostructures were attached on the blades and one disk using double-sided tape. A smooth metal rod was used as a rotation axis to assemble the hybridized TENG through the centers of the wheel blades and the two disks. The back disk and the wheel blades were connected to each other and rotated together. The front disk was fixed on the rotation axis, and kept motionless as the back disk rotated. A screw behind the back disk was used to adjust the distance between the two disks. The closer contact can induce higher effective contact area, tribo-charge density, V_{oc}, and I_{sc}, while largely increasing the rotation resistance between the two disks. In our experiment, the two disks were moderately contacted in a low rotation resistance status.

Electric Output Measurement of TENG. In the electric output measurement of the hybridized TENG, the flowing water from a household faucet or the wind from the compressed air with a flow rate controller was used to drive the rotation of the blades' wheel and the back disk. The current meter (SR570 low noise current amplifier, Stanford Research System) and voltage meter (6514 system electrometer, Keithley) were used to measure the electric outputs of the TENG.

Conflict of Interest: The authors declare no competing financial interest.

Acknowledgment. This work was supported by MURI (Airforce Researcg Lab), Office of Basic Energy Sciences (DE-FG02-07ER46394), U.S. Department of Energy, NSF, NSFC (61176067), a joint project with Sungkyunkwan University, Korea, and the "thousands talents" program for pioneer researcher and his innovation team, China, Beijing City Committee of science and technology project (Z131100006013004). Patents have been filed based on the research presented here.

Supporting Information Available: More detailed information about the electrical output of the hybridized TENG using a hydrophilic nylon film, the dependences of the open-circuit voltage and short-circuit current of the hybridized TENG on the resistance, the electrical output of the water-TENG part when it is driven by wind and there is no flowing water, and the dependences of the rotation speed of the hybridized TENG on the flowing water rate and wind speed. This material is available free of charge *via* the Internet at http://pubs.acs.org.

REFERENCES AND NOTES

1. Wang, Z. L.; Zhu, G.; Yang, Y.; Wang, S. H.; Pan, C. F. Progress in Nanogenerators for Portable Electronics. *Mater. Today* **2012**, *15*, 532–543.
2. Wang, Z. L.; Wu, W. Z. Nanotechnology-Enabled Energy Harvesting for Self-Powered Micro-/Nanosystems. *Angew. Chem., Int. Ed.* **2012**, *51*, 11700–11721.
3. Beeby, S. P.; Tudor, M. J.; White, N. M. Energy Harvesting Vibration Sources for Microsystems Applications. *Meas. Sci. Technol.* **2006**, *17*, R175–R195.
4. Mitcheson, P. D.; Yeatman, E. M.; Rao, G. K.; Holmes, A. S.; Green, T. C. Energy Harvesting from Human and Machine Motion for Wireless Electronic Devices. *Proc. IEEE* **2008**, *96*, 1457–1486.
5. Williams, C. B.; Shearwood, C.; Harradine, M. A.; Mellor, P. H.; Birch, T. S.; Yates, R. B. Development of an Electromagnetic Micro-Generator. *Proc. IEEE Circ. Dev. Syst.* **2001**, *148*, 337–342.
6. Beeby, S. P.; Torah, R. N.; Tudor, M. J.; Glynne-Jones, P.; O'Donnell, T.; Saha, C. R.; Roy, S. A Micro Electromagnetic Generator for Vibration Energy Harvesting. *J. Micromech. Microeng.* **2007**, *17*, 1257–1265.
7. Mitcheson, P. D.; Miao, P.; Stark, B. H.; Yeatman, E. M.; Holmes, A. S.; Green, T. C. MEMS Electrostatic Micropower Generator for Low Frequency Operation. *Sens. Actuators, A* **2004**, *115*, 523–529.
8. Naruse, Y.; Matsubara, N.; Mabuchi, K.; Izumi, M.; Suzuki, S. Electrostatic Micro Power Generation from Low-Frequency Vibration such as Human Motion. *J. Micromech. Microeng.* **2009**, *19*, 094002.
9. Wang, Z. L.; Song, J. H. Piezoelectric Nanogenerators Based on Zinc Oxide Nanowire Arrays. *Science* **2006**, *312*, 242–246.
10. Qin, Y.; Wang, X. D.; Wang, Z. L. Microfiber-Nanowire Hybrid Structure for Energy Scavenging. *Nature* **2008**, *451*, 809–813.
11. Chang, C. E.; Tran, V. H.; Wang, J. B.; Fuh, Y. K.; Lin, L. W. Direct-Write Piezoelectric Polymeric Nanogenerator with High Energy Conversion Efficiency. *Nano Lett.* **2010**, *10*, 726–731.
12. Chen, X.; Xu, S. Y.; Yao, N.; Shi, Y. 1.6 V Nanogenerator for Mechanical Energy Harvesting Using PZT Nanofibers. *Nano Lett.* **2010**, *10*, 2133–2137.
13. Hu, Y. F.; Lin, L.; Zhang, Y.; Wang, Z. L. Replacing a Battery by a Nanogenerator with 20 V Output. *Adv. Mater.* **2012**, *24*, 110–114.
14. Gu, L.; Cui, N. Y.; Cheng, L.; Xu, Q.; Bai, S.; Yuan, M. M.; Wu, W. W.; Liu, J. M.; Zhao, Y.; Ma, F.; *et al.* Flexible Fiber Nanogenerator with 209 V Output Voltage Directly Powers a Light-Emitting Diode. *Nano Lett.* **2013**, *13*, 91–94.
15. Park, K. I.; Lee, M.; Liu, Y.; Moon, S.; Hwang, G. T.; Zhu, G.; Kim, J. E.; Kim, S. O.; Kim, D. K.; Wang, Z. L.; *et al.* Flexible Nanocomposite Generator Made of $BaTiO_3$ Nanoparticles and Graphitic Carbons. *Adv. Mater.* **2012**, *24*, 2999–3004.

16. Fan, F. R.; Tian, Z. Q.; Wang, Z. L. Flexible Triboelectric Generator. *Nano Energy* **2012**, *1*, 328–334.
17. Fan, F. R.; Lin, L.; Zhu, G.; Wu, W. Z.; Zhang, R.; Wang, Z. L. Transparent Triboelectric Nanogenerators and Self-Powered Pressure Sensors Based on Micropatterned Plastic Films. *Nano Lett.* **2012**, *12*, 3109–3114.
18. Zhu, G.; Pan, C. F.; Guo, W. X.; Chen, C. Y.; Zhou, Y. S.; Yu, R. M.; Wang, Z. L. Triboelectric-Generator-Driven Pulse Electrodeposition for Micropatterning. *Nano Lett.* **2012**, *12*, 4960–4965.
19. Wang, S. H.; Lin, L.; Wang, Z. L. Nanoscale Triboelectric-Effect-Enabled Energy Conversion for Sustainably Powering Portable Electronics. *Nano Lett.* **2012**, *12*, 6339–6346.
20. Zhang, X. S.; Han, M. D.; Wang, R. X.; Zhu, F. Y.; Li, Z. H.; Wang, W.; Zhang, H. X. Frequency-Multiplication High-Output Triboelectric Nanogenerator for Sustainably Powering Biomedical Microsystems. *Nano Lett.* **2013**, *13*, 1168–1172.
21. Zhu, G.; Lin, Z.-H.; Jing, Q. S.; Bai, P.; Pan, C. F.; Yang, Y.; Zhou, Y. S.; Wang, Z. L. Toward Large-Scale Energy Harvesting by a Nanoparticle-Enhanced Triboelectric Nanogenerator. *Nano Lett.* **2013**, *13*, 847–853.
22. Bai, P.; Zhu, G.; Liu, Y.; Chen, J.; Jing, Q. S.; Yang, W. Q.; Ma, J. S.; Zhang, G.; Wang, Z. L. Cylindrical Rotating Triboelectric Nanogenerator. *ACS Nano* **2013**, *7*, 6361–6366.
23. Wang, S. H.; Lin, L.; Xie, Y. N.; Jing, Q. S.; Niu, S. M.; Wang, Z. L. Sliding-Triboelectric Nanogenerators Based on In-Plane Charge-Separation Mechanism. *Nano Lett.* **2013**, *13*, 2220–2225.
24. Zhu, G.; Chen, J.; Liu, Y.; Bai, P.; Zhou, Y. S.; Jing, Q. S.; Pan, C. F.; Wang, Z. L. Linear-Grating Triboelectric Generator Based on Sliding Electrification. *Nano Lett.* **2013**, *13*, 2282–2289.
25. Lin, L.; Wang, S. H.; Xie, Y. N.; Jing, Q. S.; Niu, S. M.; Hu, Y. F.; Wang, Z. L. Segmentally Structured Disk Triboelectric Nanogenerator for Harvesting Rotational Mechanical Energy. *Nano Lett.* **2013**, *13*, 2916–2923.
26. Cheng, G.; Lin, Z.-H.; Lin, L.; Du, Z. L.; Wang, Z. L. Pulsed Nanogenerator with Huge Instantaneous Output Power Density. *ACS Nano* **2013**, *7*, 7383–7391.
27. Yang, Y.; Zhang, H. L.; Chen, J.; Jing, Q. S.; Zhou, Y. S.; Wen, X. N.; Wang, Z. L. Single-Electrode-Based Sliding Triboelectric Nanogenerator for Self-Powered Displacement Vector Sensor System. *ACS Nano* **2013**, *7*, 7342–7351.
28. Yang, Y.; Zhang, H. L.; Lin, Z.-H.; Zhou, Y. S.; Jing, Q. S.; Su, Y. J.; Yang, J.; Chen, J.; Hu, C. G.; Wang, Z. L. Human Skin Based Triboelectric Nanogenerators for Harvesting Biomechanical Energy and as Self-Powered Active Tactile Sensor System. *ACS Nano* **2013**, *7*, 9213–9222.
29. Castle, G. S. P. Contact Charging between Insulators. *J. Electrostat.* **1997**, *40–41*, 13–20.
30. McCarty, L. S.; Whitesides, G. M. Electrostatic Charging due to Separation of Ions at Interfaces: Contact Electrification of Ionic Electrets. *Angew. Chem., Int. Ed.* **2008**, *47*, 2188–2207.
31. Wiles, J. A.; Grzybowski, B. A.; Winkleman, A.; Whitesides, G. M. A Tool for Studying Contact Electrification in Systems Comprising Metals and Insulating Polymers. *Anal. Chem.* **2003**, *75*, 4859–4867.
32. Lin, Z.-H.; Zhu, G.; Zhou, Y. S.; Yang, Y.; Bai, P.; Chen, J.; Wang, Z. L. A Self-Powered Triboelectric Nanosensor for Mercury Ion Detection. *Angew. Chem., Int. Ed.* **2013**, *52*, 5065–5069.
33. Lin, Z.-H.; Xie, Y. N.; Yang, Y.; Wang, S. H.; Zhu, G.; Wang, Z. L. Enhanced Triboelectric Nanogenerators and Triboelectric Nanosensor Using Chemically Modified TiO_2 Nanomaterials. *ACS Nano* **2013**, *7*, 4554–4560.
34. Yang, Y.; Zhang, H. L.; Liu, Y.; Lin, Z.-H.; Lee, S. M.; Lin, Z. Y.; Wong, C. P.; Wang, Z. L. Silicon-Based Hybrid Energy Cell for Self-Powered Electrodegradation and Personal Electronics. *ACS Nano* **2013**, *7*, 2808–2813.
35. Lin, Z.-H.; Cheng, G.; Lin, L.; Lee, S.; Wang, Z. L. Water-Solid Surface Contact Electrification and Its Use for Harvesting Liquid-Wave Energy. *Angew. Chem., Int. Ed.* **2013**, *52*, 12545–12549.
36. Lin, Z.-H.; Cheng, G.; Lee, S.; Wang, Z. L. Harvesting Water Drop Energy by a Sequential Contact-Electrification and Electrostatic-Induction Process. Unpublished work, **2014**.
37. Choi, D.; Lee, H.; Im, D. J.; Kang, I. S.; Lim, G.; Kim, D. S.; Kang, K. H. Spontaneous Electrical Charging of Droplets by Conventional Pipetting. *Sci. Rep.* **2013**, *3*, 2037.